Weierstraß-Institut
für Angewandte Analysis und Stochastik

im Forschungsverbund Berlin e.V.

Preprint ISSN 0946 – 8633

Diffusion Tensor Imaging: Structural adaptive smoothing

Karsten Tabelow[1 3], Jörg Polzehl [1], Vladimir Spokoiny [1], Henning U. Voss[2 4],

submitted: 8th June 2007

[1] Weierstrass Institute
for Applied Analysis and Stochastics,
Mohrenstr. 39, 10117
Berlin, Germany
E-Mail: tabelow@wias-berlin.de

[2] Dept. of Radiology,
Weill Medical College of Cornell University,
New York, NY, United States

No. 1232

Berlin 2007

[3]Supported by the DFG Research Center Matheon "Mathematics for key technologies" in Berlin

[4]Supported by a research grant of the Cervical Spine Research Society

2000 *Mathematics Subject Classification.* 62P10, 92C55, 62G05, 62G10 .

Key words and phrases. Diffusion tensor imaging, spatially adaptive smoothing.

Edited by
Weierstraß-Institut für Angewandte Analysis und Stochastik (WIAS)
Mohrenstraße 39
10117 Berlin
Germany

Fax: + 49 30 2044975
E-Mail: preprint@wias-berlin.de
World Wide Web: http://www.wias-berlin.de/

Abstract

Diffusion Tensor Imaging (DTI) data is characterized by a high noise level. Thus, estimation errors of quantities like anisotropy indices or the main diffusion direction used for fiber tracking are relatively large and may significantly confound the accuracy of DTI in clinical or neuroscience applications. Besides pulse sequence optimization, noise reduction by smoothing the data can be pursued as a complementary approach to increase the accuracy of DTI. Here, we suggest an anisotropic structural adaptive smoothing procedure, which is based on the Propagation-Separation method and preserves the structures seen in DTI and their different sizes and shapes. It is applied to artificial phantom data and a brain scan. We show that this method significantly improves the quality of the estimate of the diffusion tensor and hence enables one either to reduce the number of scans or to enhance the input for subsequent analysis such as fiber tracking.

1 Introduction

Since the early times of nuclear magnetic resonance, it has been known that this phenomenon is sensitive to, and thus can be used to measure, diffusion of molecules in complex systems [Carr and Purcell, 1954]. The basic principles of magnetic resonance diffusion weighted imaging (DWI) were introduced in the 1980's [Bihan and Breton, 1985, Merboldt et al., 1985, Taylor and Bushell, 1985]. Since then, DWI has evolved into a versatile tool for in-vivo examination of tissues in the human brain [Bihan et al., 2001] and spinal cord [Clark et al., 1999], leading to a plethora of clinical and neuroscience applications. The broad interest in this technique grows from the fact that DWI probes microscopic structures well beyond typical image resolutions through water molecule displacement, which can be used in particular to characterize the integrity of neuronal tissue in the central nervous system.

Diffusion in neuronal tissue is usually not isotropic but depends on the particular microscopic structure of the tissue. Different diffusion directions can be probed by application of corresponding bipolar magnetic field diffusion gradients [Stejskal and Tanner, 1965]. In diffusion tensor imaging (DTI) [Basser et al., 1994b, Basser et al., 1994a], this direction dependence is utilized to reveal information not only about local diffusivity but also local diffusion anisotropy, and thus, fiber structure. The information contained in the diffusion weighted images consists of a voxelwise integral of the microscopic diffusion properties. In DTI, this information is reduced to a three dimensional Gaussian distribution model for diffusion. Within this model, diffusion is completely characterized by the diffusion tensor, a symmetric positive definite 3×3 matrix with six independent components. This model describes diffusion completely if the microscopic diffusion properties within a voxel are homogeneous. In the presence of partial voluming effects, like crossing fibers, this model is only an approximation. For these cases, more sophisticated models exist, which include higher order tensors or describe non-Gaussian diffusion distributions, like high angular resolution diffusion imaging [Tuch et al., 1999, Frank, 2001]. In this paper, we restrict ourselves to the Gaussian diffusion tensor model for anisotropic diffusion, as used in DTI.

There are several clinical and basic neuroscience applications of DTI in the human brain. For a review, see [Sundgren et al., 2004] and [Mori and Zhang, 2006], respectively. Diffusion in brain white matter is highly anisotropic due to its organization into fibers of neuronal axons. DTI is able to reveal information on this fiber structure and on connections of the different regions in the brain [Melhem et al., 2002]. Fiber tracking has become an important field of interest, since it is possible to gain insight into the connections in the brain in vivo with applications such as surgical planning. In clinical or developmental studies, diffusion or anisotropy indices are usually compared by normalizing the brain volumes to a template before application of voxel-wise comparison tests [Schwartzman et al., 2005, Smith et al., 2006]. This way, the accuracy of diffusion and anisotropy based measures is of crucial importance, since their variability directly determines the sensitivity to detect changes over time or differences between subjects. DTI has been used in longitudinal studies and comparison of patient groups, for example in cognitive studies [Liston et al., 2006, Khong et al., 2006], developmental studies [McKinstry et al., 2002, Schneider et al., 2004, Bengtsson et al., 2005, Mukherjee and McKinstry, 2006], assessment of brain injury [Liu et al., 1999, Nakayama et al., 2006] and cancer treatment [Leung et al., 2004], or genetic studies [Carbon et al., 2004, O'Sullivan et al., 2005]. All these studies have in common that subtle changes in diffusion or anisotropy in white matter brain areas were used as an indicator for neuronal changes or differences.

DTI suffers from significant noise which may render subsequent analysis or medical decisions more difficult. This is especially important since it has been shown that noise may induce a systematically biased assessment of features. For example, a well known phenomenon is the biased estimation of anisotropy indices in the presence of noise [Basser and Pajevic, 2000, Hahn et al., 2006]. At high noise levels, in addition to the common random errors, the order of the diffusion eigenvectors is subject to a sorting bias.

Noise reduction is therefore essential. Several approaches have been proposed for smoothing diffusion tensor data. They include common methods such as Gaussian smoothing [Westin et al., 1999], anisotropic kernel estimates [Lee et al., 2005], and methods based on non-linear diffusion [Weickert, 1998, Weickert, 1999, Parker et al., 2000, Ding et al., 2005] or splines [Heim et al., 2007]. In general, due to the bias introduced by noise, it is essential to apply the smoothing directly to the images rather than to the direction field of the principal tensor eigenvectors or the tensor field. This is even more advisable since operation in tensor space involves serious mathematical difficulties in choosing the appropriate metric [Fletcher, 2004].

Here, we propose a new method based on the Propagation-Separation (PS) approach [Polzehl and Spokoiny, 2006]. By naturally adapting to the structures of interest at different scales, the algorithm avoids loss of information on size and shape of structures, which is typically observed when using non-adaptive filters. More specific, by virtue of inspecting scale space in an iterative way, PS accumulates information on the spatial structure at small scales and uses this information to improve estimates at coarser scales.

This article is organized as follows: In section 2 we briefly review the basic notation of DTI and smoothing methods. Section 3 is dedicated to our structural adaptive smoothing algorithm based on the propagation-separation approach. We apply the method to artificial as well as experimental data in section 4. The last section 5 summarizes and discusses our results.

2 Diffusion Tensor Imaging

2.1 Diffusion Tensor

Let $S_{\vec{b}}$ denote the diffusion weighted image acquired when applying the magnetic field gradient in direction $\vec{b}$ with the "b-value" b. S_0 corresponds to the non-diffusion weighted image ($b = 0$). As an effect of the diffusion of molecules in the gradient direction $\vec{b}$, the signal $S_{\vec{b}}$ is attenuated relative to S_0 approximately in an exponential way, i.e.,

$$S_{\vec{b}} = S_0 \exp(-bD(\vec{b})) \,, \tag{1}$$

where $D(\vec{b})$ is the diffusion constant with respect to the applied gradient. Using a Gaussian model of diffusion, the anisotropy can be modeled by a diffusion tensor, which is represented by a symmetric positive definite 3×3 matrix:

$$\mathcal{D} = \begin{pmatrix} D_{xx} & D_{xy} & D_{xz} \\ D_{xy} & D_{yy} & D_{yz} \\ D_{xz} & D_{yz} & D_{zz} \ . \end{pmatrix} \tag{2}$$

Therefore, the "b-value" in Eq.(1) is replaced by a "b-matrix" [Mattiello et al., 1994, Mattiello et al., 1997].

To completely determine the diffusion tensor, one has to acquire diffusion weighted images for at least 6 gradient directions $\vec{b}$. $\mathcal{D}$ can be estimated e.g. via multiple linear regression. The tensor components depend on the orientation of the object in the scanner frame xyz. To circumvent this dependence, only rotationally invariant quantities derived from the diffusion tensor are usually used for further analysis, for example the eigenvalues and eigenvectors.

The diffusion tensor can be represented by a diffusion ellipsoid where the three main axis represent the eigenvalues of the tensor, μ_i $(i = 1, 2, 3)$. The principal eigenvalue μ_1 and the corresponding eigenvector determine the main diffusion direction. Since the eigenvalues are rotationally invariant, quantities based on these can be properly defined. One of these invariant quantities is the trace of the diffusion tensor

$$Tr(\mathcal{D}) = \mu_1 + \mu_2 + \mu_3 \ . \tag{3}$$

The value $\langle\mu\rangle = Tr(D)/3$ is called mean diffusivity and completely neglects the anisotropy of the diffusion. Another very commonly used parameter is the fractional anisotropy (FA), which is based on second order moments of the eigenvalues, and is defined as

$$FA = \sqrt{\frac{3}{2}} \sqrt{\frac{(\mu_1 - \langle\mu\rangle)^2 + (\mu_2 - \langle\mu\rangle)^2 + (\mu_3 - \langle\mu\rangle)^2}{\mu_1^2 + \mu_2^2 + \mu_3^2}} \ . \tag{4}$$

Higher moments can be used for more complete characterization of anisotropy (such as skewness or kurtosis) [Westin et al., 1999, Alexander et al., 2000].

Note that the estimation errors of the eigenvalues are not rotationally invariant. About 30 gradient directions are required for robust quantitative measurements of eigenvalues and tensor orientation [Jones, 2003, Jones, 2004]. Therefore, to decrease estimation errors, in practice one measures more than 6 directions [Kinglsey, 2006], however, at the cost of acquisition time.

2.2 Smoothing diffusion tensor data

Due to the diffusion attenuation in the diffusion weighted images, the fact that white matter appears already with low intensity in T2 weighted images, and its high motion sensitivity, DTI suffers from significant noise. This is even more serious, as DTI probes microscopic structures well below typical voxel sizes, causing intra-voxel dephasing. Noise in the diffusion weighted images is reflected as noise in the estimated diffusion tensor and subsequently all derived quantities. Additionally, it has been shown [Basser and Pajevic, 2000, Hahn et al., 2006], that the estimates of the tensor and derived quantities are intrinsically biased. This bias depends on the signal size S and the noise variance.

Figure 1a,b shows the influence of relatively strong noise on the direction field of principal eigenvectors. It is evident that the direction field is irreversibly corrupted by noise. There-

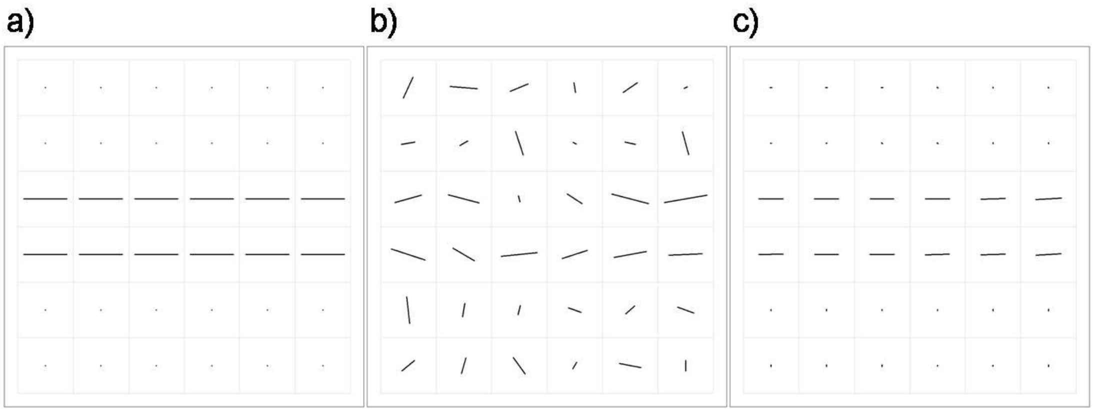

Figure 1: Effect of noise in the diffusion weighted images on the direction field of principal eigenvectors. (a) An artificial 3D DTI dataset has been created based on the direction field shown in the left figure. The direction of the lines corresponds to the direction of the direction field whereas the length of the lines corresponds to the anisotropy (FA = 0 and 0.8 for the dots and lines, respectively). One slice is shown. (b) The direction field for noisy images. Smoothing the direction field (and not the original images) can therefore only be of limited use. (c) The direction field after smoothing the original images with the here proposed method.

fore, smoothing algorithms that operate on the FA-map or the direction field itself such as in [Koltchinskii et al., 2007] can only be of limited use. In addition, those algorithms cannot improve the bias of the estimated diffusion tensor, and smoothing the tensor field itself requires choice of an appropriate metric [Fletcher, 2004]. We therefore suggest to smooth the diffusion weighted images. This has already been done using non-linear diffusion methods [Parker et al., 2000, Ding et al., 2005] or splines [Heim et al., 2007]. Here, we use the Propagation-Separation approach which has been successfully applied to the analysis of fMRI data [Tabelow et al., 2006b, Tabelow et al., 2006a, Voss et al., 2007]. An application of this method to the artificial dataset is shown in Fig. 1c.

3 Structural Adaptive Smoothing of DTI data

The main idea of the proposed approach is to reduce the error of estimating the tensor directions and tensor characteristics like fractional anisotropy by a preliminary smoothing of the observed DTI data. The application of a standard Gauss filtering would be highly inefficient in the DTI applications in view of the anisotropic nature of the diffusion tensor. Indeed, the tensor direction remain constant only along the fiber directions and averaging over a large symmetric neighborhood of every voxel would lead to the lost of directional information.

Our underlying structural assumption is that for every voxel there is a neighborhood of this voxel in which the diffusion tensor is nearly constant. This assumption reflects the fact that the structures of interest are regions with a homogeneous fractional anisotropy, a homogeneous diffusivity, and a locally constant direction field. The shape of this neighborhood can be quite different for different points and cannot be described by few simple characteristics like bandwidth or principal directions. The PS approach from [Polzehl and Spokoiny, 2006] is specially developed for dealing with spatial structures with unknown shape. It describes the local neighborhood of homogeneity around every voxel by means of a collection of nonnegative weights. However, the original proposal from [Polzehl and Spokoiny, 2006] is only applicable to denoising the usual images or sequences of images, [Tabelow et al., 2006b]. An extension of this proposal to the DTI is a nontrivial task because it requires to compare estimated local DTI structures at different voxels.

3.1 Propagation-Separation approach

Let us assume that for each voxel with coordinates $i = (i_x, i_y, i_z)$, the expected values of the diffusion weighted signal $S_{\vec{b},j}$ and the non-diffusion weighted signal $S_{0,j}$ within a local vicinity $j \in \mathcal{U}(i)$ of voxel i can approximately be described by a constant, i.e.

$$\boldsymbol{E} S_{\vec{b},j} = \boldsymbol{E} S_{\vec{b},i} \quad \forall \vec{b} \quad \forall j \in \mathcal{U}(i). \tag{5}$$

Discontinuities in any of the diffusion weighted images $S_{\vec{b}}$ result in discontinuities for the diffusion tensor. We therefore assume that within $\mathcal{U}(i)$ the diffusion tensor is homogeneous.

In order to estimate the diffusion weighted signal $S_{\vec{b},i}$ (as well as $S_{0,i}$), we define local weights $W_i = \{w_{i1}, \ldots, w_{in}\}$ (n the number of voxels). In contrast to non-adaptive weighting schemes, which depend on some fixed bandwidth and kernel function, we determine

W_i for each voxel i from the data to reflect the local homogeneity structure given by $\mathcal{U}(i)$. If we knew the neighborhood $\mathcal{U}(i)$, we could define local weights as $w_{ij} = I_{j\in\mathcal{U}(i)}$ and use the weighted least squares estimate

$$\widehat{S}_{\vec{b},i} = \sum_j w_{ij} S_{\vec{b},j} / \sum_j w_{ij} \tag{6}$$

as an estimate of $\boldsymbol{E}S_{\vec{b},i}$. From this we could get an improved estimate $\widehat{\mathcal{D}}_i$ for the diffusion tensor from

$$-\ln \frac{\widehat{S}_{\vec{b},i}}{\widehat{S}_{0,i}} = \vec{\mathbf{b}}\vec{\mathcal{D}} + \varepsilon_{\vec{b},i} \ , \tag{7}$$

with matrix $\mathbf{b} = \vec{b}\ \vec{b}^\top$ and tensor $\mathcal{D}$ vectorized as $\vec{\mathbf{b}} = (b_{xx}, b_{yy}, b_{zz}, 2b_{xy}, 2b_{xz}, 2b_{yz})^\top$ and $\vec{\mathcal{D}} = (D_{xx}, D_{yy}, D_{zz}, D_{xy}, D_{xz}, D_{yz})^\top$, respectively. The error $\varepsilon_{\vec{b},i}$ is considered to be Gaussian $\mathcal{N}(0, \sigma_i)$, although realistic noise is more complicated due to the nonlinearities in Eq. (7) [Hahn et al., 2006]. An estimate $\widehat{\sigma}_i^2$ for σ_i^2 can be obtained from the residuals of the linear model Eq. (7). Hence, we have

$$\operatorname{Var} \widehat{\vec{\mathcal{D}}}_i = \sigma_i^2 \mathcal{B} \ , \tag{8}$$

where $\mathcal{B} = \sum_{\mathbf{b}} \vec{\mathbf{b}}\vec{\mathbf{b}}^\top$ [Mattiello et al., 1994, Mattiello et al., 1997]. Since the homogeneity structure is defined from the diffusion tensor, we use the same weighting scheme W_i for obtaining estimates $\widehat{S}_{\vec{b}}$ for all diffusion weighted images.

However, the neighborhoods $\mathcal{U}(i)$ are unknown and hence must be determined from the data. If we had estimates of $\widehat{S}_{\vec{b},i}$, we could decide whether j belongs to the set $\mathcal{U}(i)$ by testing the hypothesis

$$H : \boldsymbol{E}S_{\vec{b},i} = \boldsymbol{E}S_{\vec{b},j} \quad \forall \vec{b} \ . \tag{9}$$

Due to the high dimensionality of the space of diffusion weighted images, a test simply based on the Euclidian distance would be highly inefficient [Neyman, 1937, Fan, 1996]. A much more efficient test can be derived using an informative sub-space. Since the information we are interested in is contained in the diffusion tensor itself, a natural test statistic is

$$T_{ij} = \frac{1}{\widehat{\sigma}_i^2} (\widehat{\vec{\mathcal{D}}}_i - \widehat{\vec{\mathcal{D}}}_j) \mathcal{B}^{-1} (\widehat{\vec{\mathcal{D}}}_i - \widehat{\vec{\mathcal{D}}}_j)^\top \ . \tag{10}$$

This basically amounts in testing the hypothesis

$$H' : \mathcal{D}_i = \mathcal{D}_j \ . \tag{11}$$

Based on the value of T_{ij}, we can refine the non-adaptive weighting scheme W_i and assign zero weights if $\mathcal{D}_i$ and $\mathcal{D}_j$ are significantly different. This corrected weighting scheme reflects the homogeneity structure $\mathcal{U}(i)$ and can be used to obtain new estimates of $\boldsymbol{E}S_{\vec{b},i}$ and hence $\mathcal{D}$ in each voxel i by Eqns. (6) and (7) .

We utilize both steps, estimation of parameters and testing homogeneity, in an iterative procedure. Iteration starts at step 0 with a very local model in each voxel i given by weights

$$w_{ij}^{(0)} = \delta_{ij} \ ,$$

where δ_{ij} is Kronecker's delta symbol. The initial estimates $\widehat{S}_i$ using Eq. (6) therefore coincide with the data.

We now generate a geometric series $(h^{(k)})_{k=0,\cdots,k^*}$ of bandwidths. First, an anisotropic metric

$$\Delta^2(i,j,\mathcal{D}) = \det \mathcal{D} \begin{pmatrix} i_x - j_x \\ i_y - j_y \\ i_z - j_z \end{pmatrix}^\top \mathcal{D}^{-1} \begin{pmatrix} i_x - j_x \\ i_y - j_y \\ i_z - j_z \end{pmatrix} \tag{12}$$

is defined. It enables us to use the anisotropy information contained in the diffusion tensor itself by inserting a regularized estimate of the diffusion tensor, $\widetilde{\mathcal{D}}$. Defining weights as

$$\widetilde{w}_{ij}^{(k)} \quad = \quad K_{\mathrm{loc}}(\Delta(i,j,\widetilde{\mathcal{D}}_i^{(k-1)})/h^{(k)}) \tag{13}$$

leads to series of anisotropic kernel estimates similar to [Chung et al., 2005, Lee et al., 2005].

Let $W_i^{(k-1)}$ be the weighting scheme from step $k-1$. We can then use the homogeneity information available from $\widehat{\mathcal{D}}^{(k-1)}$ by introducing a statistical penalty

$$s_{ij}^{(k)} = N_i^{(k-1)} T_{ij}^{(k)} / \lambda \tag{14}$$

with $N_i^{(k-1)} = \sum_j w_{ij}^{(k-1)}$ and a positive real control parameter λ, which is the main parameter in our approach. The choice of λ will be explained in Subsection 3.3. In the kth iteration, new weights are generated as

$$w_{ij}^{(k)} \quad = \quad K_{\mathrm{loc}}(\Delta(i,j,\widetilde{\mathcal{D}}_i^{(k-1)})/h^{(k)}) K_{\mathrm{st}}(s_{ij}^{(k)}) \ . \tag{15}$$

Both K_{loc} and K_{st} are monotone non-decreasing kernels with compact support on $[-1;1]$. The regularized tensor estimate used in Eq. (13) is given by

$$\widetilde{\mathcal{D}}_i^{(k-1)} = \widehat{\mathcal{D}}_i^{(k-1)} + \frac{\rho}{\sqrt{N_i^{(k-1)}}} I \ , \tag{16}$$

depending on a regularization parameter ρ and the sum of weights $N_i^{(k-1)}$, which characterizes the variability of the estimated tensor.

Then we recompute the estimates employing the just defined weights as

$$\widehat{S}_{\vec{b}i}^{(k)} = \frac{1}{N_i^{(k)}} \sum_j w_{ij}^{(k)} S_{\vec{b},j} \ . \tag{17}$$

The resulting procedure is essentially a multiscale procedure. In each iteration we allow for a different amount of smoothing by increasing the bandwidth $h^{(k)}$. The resulting weighting scheme excludes observations in voxel j from being used in estimates at voxel i as soon as they are detected to behave significantly different. With a high probability, such decisions are retained within the following iterations. We refer to [Polzehl and Spokoiny, 2006] for detailed properties of the weighting scheme.

3.2 Effect of spatial correlation

DTI data inherently contain spatial correlation. The statistical penalty s_{ij} effectively measures the probability of observing the estimate $\widehat{\mathcal{D}}_i$ if the correct diffusion tensor $\mathcal{D}_i$ equals $\widehat{\mathcal{D}}_j$. The penalty heavily depends on a correct assessment of the variability of $\widehat{\mathcal{D}}_i$. In case of (positive) spatial correlation the variance reduction achieved will be reduced and therefore we need to adjust the statistical penalty.

As a rough model we assume the spatial correlation to be caused by convolution with a Gaussian kernel K_G with unknown bandwidths $g = (g_x, g_y, g_z)$. This leads to a multiplicative correction factor

$$C_i(g, h) = \frac{\sum_l \left[\sum_j K_{\mathrm{loc}}(\Delta(i, j, \widetilde{\mathcal{D}}_i)/h) K_G(\Delta(i, j, \mathcal{I}_g)/(g_x g_y g_z)) \right]^2}{\sum_j K_{\mathrm{loc}}(\Delta(i, j, \widetilde{\mathcal{D}}_i)/h)^2 \quad \sum_j K_G(\Delta(i, j, \mathcal{I}_g)/(g_x g_y g_z))^2} \quad , \tag{18}$$

with $\mathcal{I}_g = diag(g)$, in the statistical penalty. For the first introduction of this correction factor see [Tabelow et al., 2006b].

3.3 Choice of parameters - Propagation Condition

The proposed procedure involves several parameters. The most important one is the control parameter λ, which appears as a scale parameter in the statistical penalty s_{ij}. The special case $\lambda = \infty$ simply leads to an adaptive anisotropic kernel estimate with bandwidth $h^{(k^*)}$ and anisotropic kernel determined by $\widehat{\mathcal{D}}_i^{(k^*-1)}$. We propose to choose the control parameter λ as the smallest value satisfying a propagation condition. This condition requires that, if the local assumption is valid globally, i.e., $\mathcal{D}_i \equiv \mathcal{D}$ does not depend on i, then with high probability the final estimate for $h_{\max} = \infty$ coincides in every point with the global estimate. Since the estimate of the diffusion tensor itself is biased, with bias depending on the mean and variance of S_0 and S_b, we formulate the propagation condition in terms of the estimated diffusion weighted images. More formally, we request that in this case for each iteration k and arbitrary $\mathcal{D}$ and S_0

$$\boldsymbol{E}|\widehat{S}_0^{(k)} - \boldsymbol{E}S_0| < (1+\alpha)\boldsymbol{E}|\check{S}_0^{(k)} - \boldsymbol{E}S_0| \tag{19}$$

for a specified constant $\alpha > 0$, where $\check{S}_0^{(k)}$ is the nonadaptive estimate obtained employing weights

$$w_{ij}^{(k)} \quad = \quad K_{\mathrm{loc}}(\Delta(i,j,\widetilde{\mathcal{D}}_i^{(k-1)})/h^{(k)})\ . \tag{20}$$

and Eq. (6). Note that this also guarantees a similar condition for the estimates of $\boldsymbol{E}S_b$ due to the use of the same weighting schemes. The value α characterizes a maximal loss in efficiency of the adaptive estimate compared to its non-adaptive counterpart, with $\alpha = 0.2$ providing reasonable results.

The control parameter λ provided by this condition is characteristic for the selected class of error distributions. A default value for λ can therefore be selected by simulations using artificial DTI data with independent Gaussian noise on structureless diffusion weighted images. In general there is no need to adjust this parameter for any experimental DTI dataset if the noise is Gaussian.

The second parameter of interest is the maximal bandwidth $h^{(k^*)}$ and hence the number of iterations k^*, which controls both numerical complexity of the algorithm and smoothness within homogeneous regions. The maximal bandwidth can be chosen by heuristic arguments, including the amount of computing time, the maximal size of homogeneous regions within the image, and the variance reduction aspired. The separation property of the procedure secures that, up to a constant factor, the quality of reconstruction reached at any intermediate step will not be lost for larger bandwidths [Polzehl and Spokoiny, 2006].

Additionally, we specify a number of parameters and kernel functions that have less influence on the resulting estimates. As a default, the kernel functions are chosen as

$$K_{\mathrm{loc}}(x,p) = K_{\mathrm{st}}(x,p) = \left\{ \begin{array}{ll} 1 & x < p \\ \frac{x-p}{1-p} & p \le x \le 1 \\ 0 & x > 1 \end{array} \right\} . \tag{21}$$

The initial bandwidth is chosen as $h^{(0)} = 1$. The bandwidth is increased after each iteration by a default factor $c_h = 1.25^{1/2}$. $p = 0.25$.

The regularization parameter ρ from Eq.(16) should be chosen such that at early steps the anisotropy in the location penalty is small, whereas at final steps with stabilized tensor estimates, the regularization has less effect.

3.4 Propagation-Separation algorithm for DTI data

We describe the adaptive smoothing algorithm briefly.

- **Initialization:** Generate $\mathcal{B} = \sum_{\mathbf{b}} \vec{\mathbf{b}}\vec{\mathbf{b}}^\top$ from gradient directions $\mathbf{b} = \vec{b}\,\vec{b}^\top$, $\vec{\mathbf{b}} = (b_{xx}, b_{yy}, b_{zz}, 2b_{xy}, 2b_{xz}, 2b_{yz})^\top$. Set $k = 0$, initialize the bandwidth $h^{(0)} = 1$ and the estimates for the diffusion weighted images

$$\widehat{S}_i^{(0)} = S_i \ ,$$

  and compute the diffusion tensor estimates $\widehat{\mathcal{D}}_i^{(0)}$ as well as $\widehat{\sigma}^{(0)}$ from Eq. (7). Set $N_i^{(0)} = 1$, $k = 1$ and $h^{(1)} = c_h h^{(0)}$.

- **Adaptation:** For every pair i, j, we compute the penalty

$$s_{ij}^{(k)} \quad = \quad \frac{N_i^{(k-1)}}{\lambda C_i(g, h^{(k-1)})\widehat{\sigma}_i^2}(\vec{\widehat{\mathcal{D}}}_i - \vec{\widehat{\mathcal{D}}}_j)\mathcal{B}^{-1}(\vec{\widehat{\mathcal{D}}}_i - \vec{\widehat{\mathcal{D}}}_j)^\top \ .$$

  Weights are computed as

$$w_{ij}^{(k)} = K_{\mathrm{loc}}\big(\Delta(i, j, \widetilde{\mathcal{D}}_i^{(k-1)})/h^{(k)}\big)K_{\mathrm{st}}\big(s_{ij}^{(k)}\big) \ ,$$

  using regularized tensor estimates $\widetilde{\mathcal{D}}_i^{(k-1)} = \widehat{\mathcal{D}}_i^{(k-1)} + \frac{\rho}{\sqrt{N_i^{(k-1)}}} I$.

- **Estimation of diffusion weighted images:** Updated local MLE estimates $\widehat{S}_{\vec{b},i}^{(k)}$ and $\widehat{S}_{0,i}^{(k)}$ of $\boldsymbol{E}S_{\vec{b},i}$ and $\boldsymbol{E}S_{0,i}$ are obtained as

$$\widehat{S}_{\vec{b},i}^{(k)} = U_{\vec{b},i}^{(k)}/N_i^{(k)}, \qquad \widehat{S}_{0,i}^{(k)} = U_{0,i}^{(k)}/N_i^{(k)} \ ,$$

  with $N_i^{(k)} = \sum_j w_{ij}^{(k)}$, $U_{\vec{b},i}^{(k)} = \sum_j w_{ij}^{(k)} S_{\vec{b},j}$ and $U_{0,i}^{(k)} = \sum_j w_{ij}^{(k)} S_{0,j}$.

- **Tensor estimation:** Estimate $\widehat{\mathcal{D}}_i^{(k)}$ and $\widehat{\sigma}^{(k)}$ from

$$-\ln \frac{\widehat{S}_{\vec{b},i}^{(k)}}{\widehat{S}_{0,i}^{(k)}} = \vec{\mathbf{b}}\vec{\mathcal{D}} + \varepsilon_{\vec{b}i}^{(k)} \ .$$

- **Stopping:** Stop if $k = k^*$, otherwise set $h^{(k+1)} = c_h h^{(k)}$, increase k by 1 and continue with the adaptation step.

4 Examples

4.1 Numerical phantom

We constructed a numerical phantom by defining a series of isocentric cylindrical shells with variable directionality and anisotropy. The phantom mimics typical situations observed in the brain parenchyma, cerebrospinal fluid (CSF), and background. It is described in detail in Fig. 2. Figure 2a shows the FA map of a slice in the x-y plane through the phantom, computed from a noise-free data set. Figures 2b–e show corresponding unrolled cylindrical shells, starting with the innermost shell and proceeding to the outermost shell. Noise was added to the phantom by transforming the T2 and diffusion weighted volumes slice-wise (in the xy plane) to k-space and adding Gaussian noise to both the real and imaginary part. The volumes where then slice-wise backtransformed into image space. Figures 2f–j show the same slice as Fig. 2a–e but computed from noisy data, and Figs. 2k–o show the result after smoothing with the proposed method. As a result, the shape of the phantom could be recovered well from the noisy data (Fig. 2k), the blurred areas in Fig. 2g appear to be distinct again (Fig. 2l), regions with different direction fields and FA inhomogeneity could be recovered well (Fig. 2m–o), the CSF compartment appears to be homogenous again (Fig. 2k, black area between the cylindrical shells), and, finally, the problem of negative eigenvalues as evident as black spots in Figs. 2f–j has been overcome.

Note that the expected intensity values in the noisy diffusion weighted images are larger than the corresponding values in the true S_0 and S_b volumes. Therefore, there are two sources of bias in the estimated tensor. The first part is caused by the positive bias of the observed S_0 and S_b images. This intrinsic bias can only be removed by a bias correction for the observed S_0 and S_b images. The second contribution to the bias comes from the nonlinear transformation in Eq. (7). This bias part is caused by variance of the observed images and can be reduced by adequate smoothing procedures. In order to illustrate this effect, we report numerical results for the FA values with respect to the tensor $\check{\mathcal{D}}$ obtained from the expected $\boldsymbol{E}S_0$ and $\boldsymbol{E}S_b$ volumes by Eq. (7) rather than the tensor defining the phantom.

To better quantify the effects of our proposed smoothing method, we computed boxplots of absolute errors of the estimated FA and deviations between the estimated FA and the FA obtained from $\check{\mathcal{D}}$, see Figs. 3a–b. These values were only computed for voxels inside the phantom. The absolute error in FA was reduced by $70 - 90\%$. Figures 3a–b show an significant reduction in the variance and an almost complete elimination of the bias

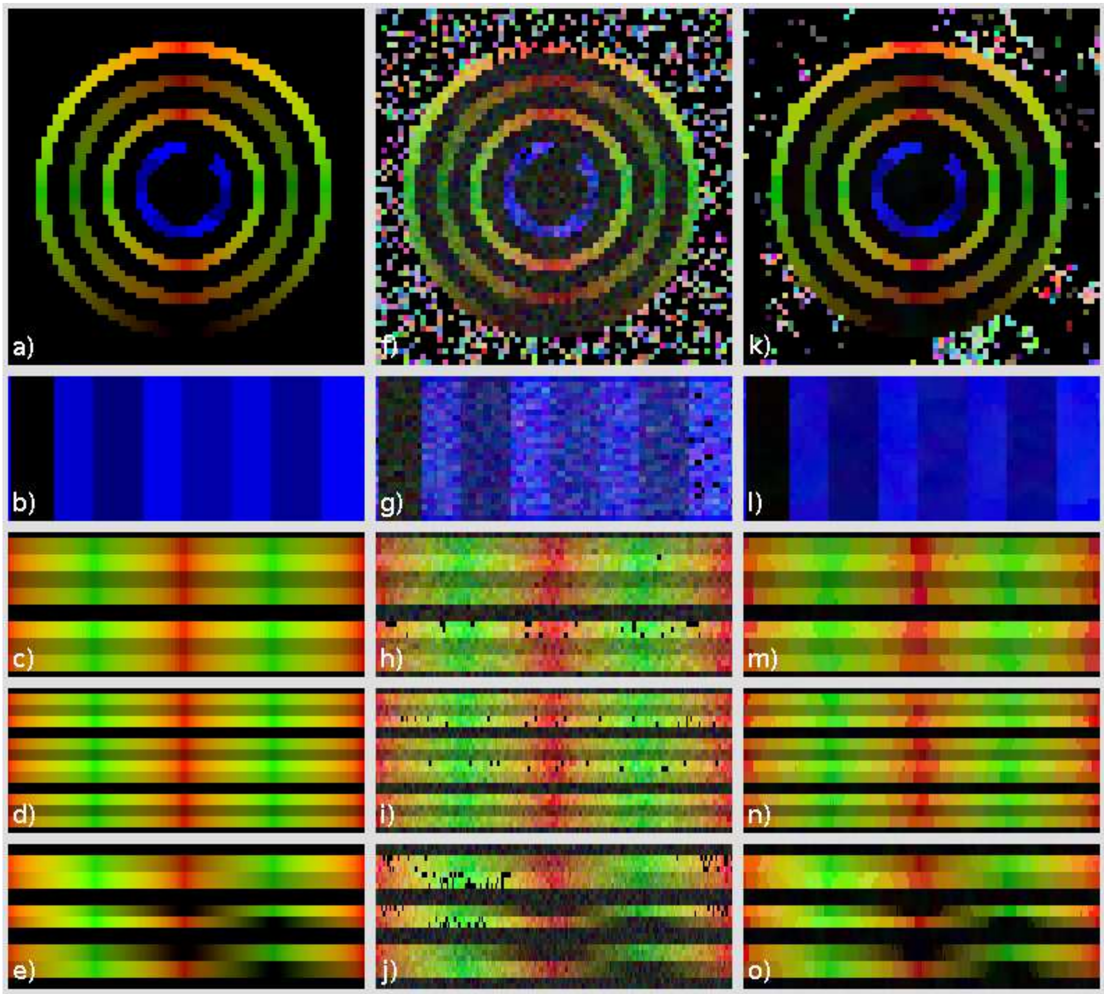

Figure 2: Reconstruction of a numerical DTI phantom of 64 × 64 × 26 voxels. The phantom consists of 4 centered cylindrical shells. The innermost shell contains eight homogeneous segments with a diffusion tensor pointing in z-direction. The second and third shell are characterized by regions with zero z-component in the tensor and constant anisotropy index (FA) within slices. The outermost shell again contains tensors with zero z-component but smoothly varying anisotropy index. Empty space between the cylinder shells and in the center is characterized by an isotropic tensor and a true S_0 value of 2500. Outside the phantom the true S_0 value is set to zero. The S_0-value within the cylindrical shells decreases with the FA-value. Noisy S_b and S_0 images are generated using the diffusion tensor model and adding noise with standard deviation 1600 to both the real and imaginary part in k-space.

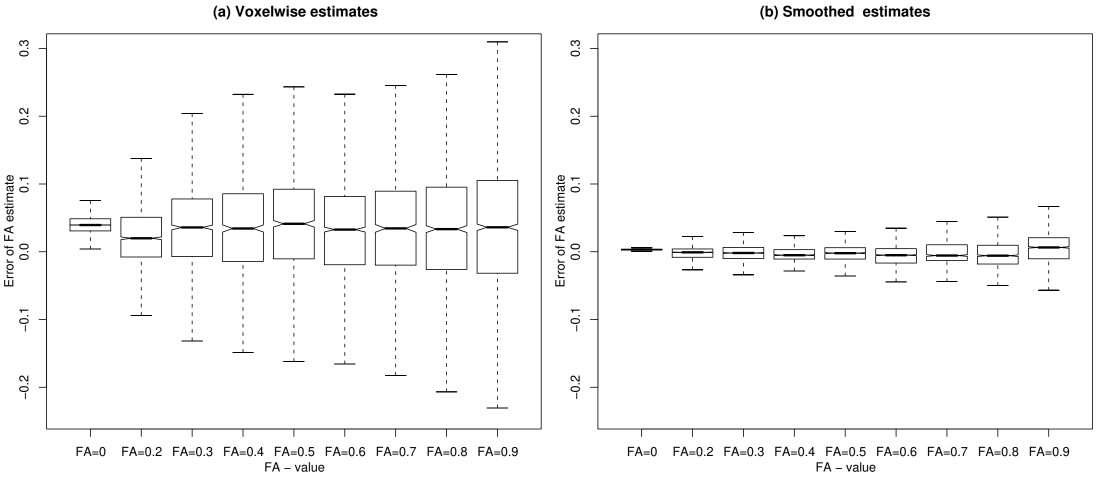

Figure 3: Boxplots of errors of the estimated FA with respect to the FA obtained from $\boldsymbol{E}S_0$ and $\boldsymbol{E}S_b$ volumes for different true FA-values. (a) Errors in FA for voxelwise estimates. (b) Errors in FA for smoothed (PS) estimates.

component caused by noise variability in the diffusion weighted images.

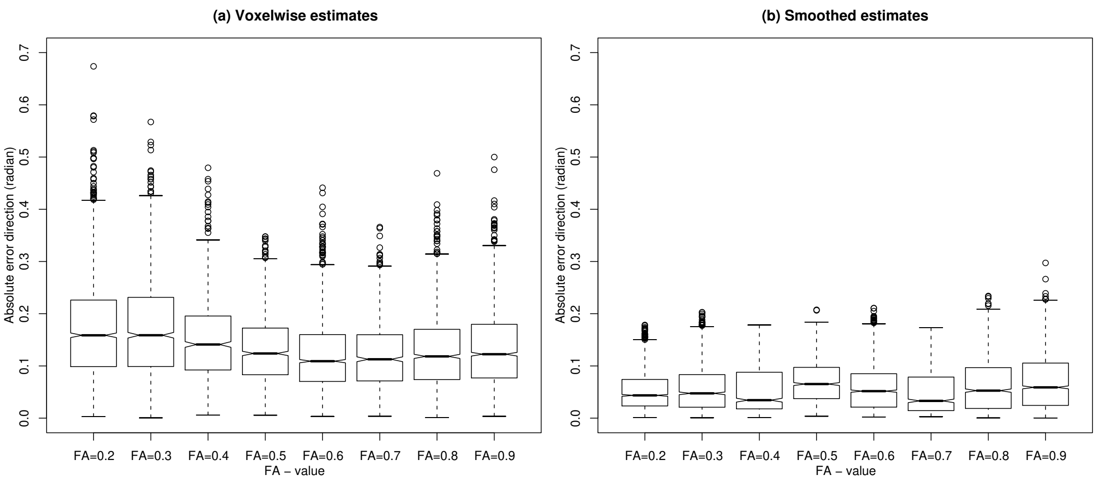

Figure 4: Boxplots of errors of the estimated principal direction measured in radians. (a) Voxelwise estimates, (b) smoothed (PS) estimates.

Figures 4a–b provide corresponding results for the estimated principal diffusion direction. The absolute direction error was defined as the mean of the absolute angles between the true (from the noise free phantom) and the estimated direction, modulo 90 degrees. We observe a mean reduction of the directional error by $50 - 70\%$.

In order to investigate the effect of the number of diffusion weighted images used, we ob-

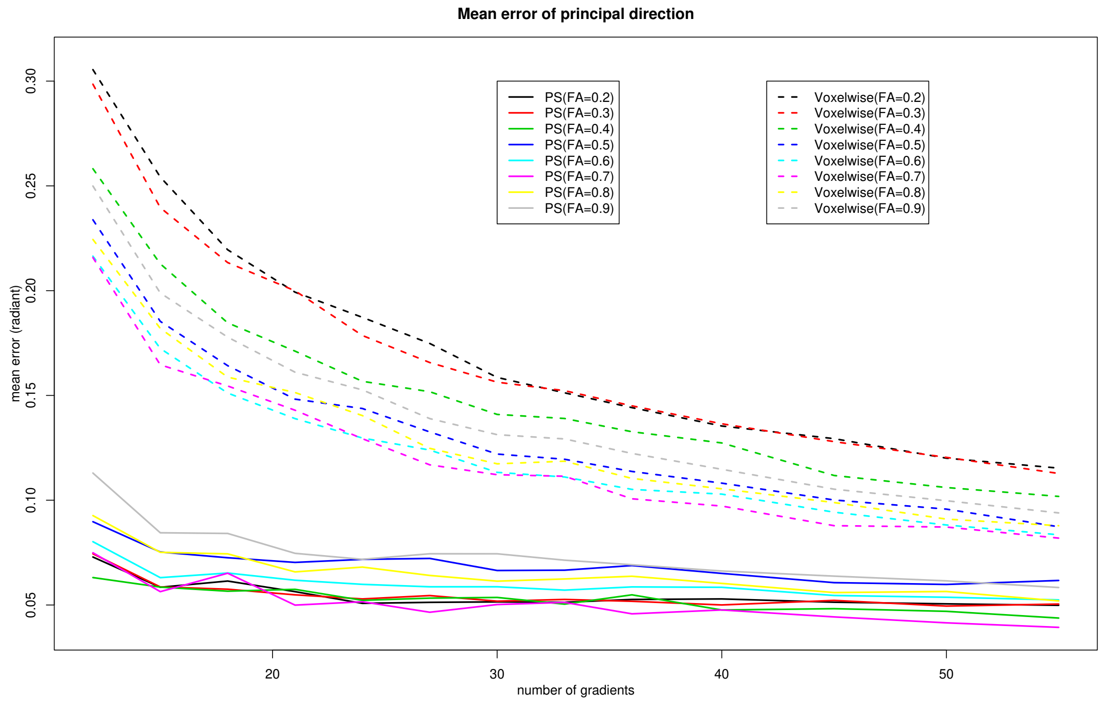

Figure 5: Absolute error of estimated principal direction as a function of the number of gradients. Gradient directions have been obtained to maximize the mean distance of gradient directions to their three neighboring directions for number of gradients equal to 12, 15, 18, 21, 24, 27, 30, 33, 36, 40, 45, 50 and 55. Solid lines correspond to errors of principal directions for PS estimates as a function of the number of gradients used, while dashed lines show the same information for voxelwise estimates. Curves for different FA-values are obtained from regions of constant FA-values within the phantom.

tained sets of gradient directions by numerically optimizing the mean distance of gradient directions to their three neighboring directions. This was done for 12, 15, 18, 21, 24, 27, 30, 33, 36, 40, 45, 50 and 55 gradients, respectively. The mean error of the estimated principal direction was then obtained for varying number of gradients by simulation based on our phantom. Figure 5 provides curves for smoothed (solid lines) and voxelwise (dashed lines) estimates and different FA-values. The figure suggests that a small number of gradients together with spatially adaptive smoothing as proposed in this paper allows for improved results compared to using a large number of gradients and voxelwise estimates.

4.2 Brain scan

Next, the procedure is applied to the DTI data of the brain of a normal volunteer. (The imaging parameters were as follows: We utilized parallel imaging on an 8-channel brain coil (acceleration factor of 2), on a 3.0 Tesla General Electric Excite MRI scanner. We used a single-shot spin-echo EPI sequence with one image without diffusion weighting and 55 diffusion gradient directions, which were approximately isotropically distributed over the sphere. Echo and repeat time were TE = 68.3 ms, TR = 7000 ms, respectively, and 72 axial slices with a matrix size of 128 $\times$ 128 were acquired. Images were zero filled to a matrix size of 256 $\times$ 256, yielding a resolution of 0.82 $\times$ 0.82 $\times$ 1.8 mm^3. The b-value in the diffusion weighted images was 1000 s/mm^2. The subject provided written informed consent in compliance with the institutional review board of Weill Medical College of Cornell University.)

Figure 6a shows a corresponding FA direction map of a medial axial slice through the brain. Figure 6c shows an FA direction map of the same brain volume which was computed from only 30 (instead of all 55 measured) diffusion images. For comparison, Figs. 6b and 6d show FA direction maps of the smoothed data ($\lambda = 25$) corresponding to Figs. 6a and 6c, respectively. It can be seen that smoothing the DTI images with PS preserves white matter structures well, without evident blurring. Furthermore, smoothing the volume that was acquired with only 30 gradient directions (Fig. 6d) achieves a less noisy FA direction map than the un-smoothed analysis using all 55 measured gradients (Fig. 6c), without evident loss of structure. These results are in accordance with the phantom results as described before. Although we do not have a gold standard of the brain scan here, it can be assumed, therefore, that the benefits of smoothing include a lower directional and FA variability and bias, without loss of white matter structures.

5 Summary and Conclusions

This paper presents a new anisotropic structural adaptive approach for smoothing diffusion weighted images. The procedure is entirely data driven and focuses on homogeneity of the diffusion tensor along its principal direction. We demonstrate, using phantom and experimental data, that the proposed procedure allows for a significant decrease of both the error in the estimated FA and in the estimate of the principal direction of the tensor. The gain in efficiency allows for providing the same accuracy with considerably less gradient directions, leading to possibly shorter acquisition times.

The method in its form as described here puts equal value on all six tensor components.

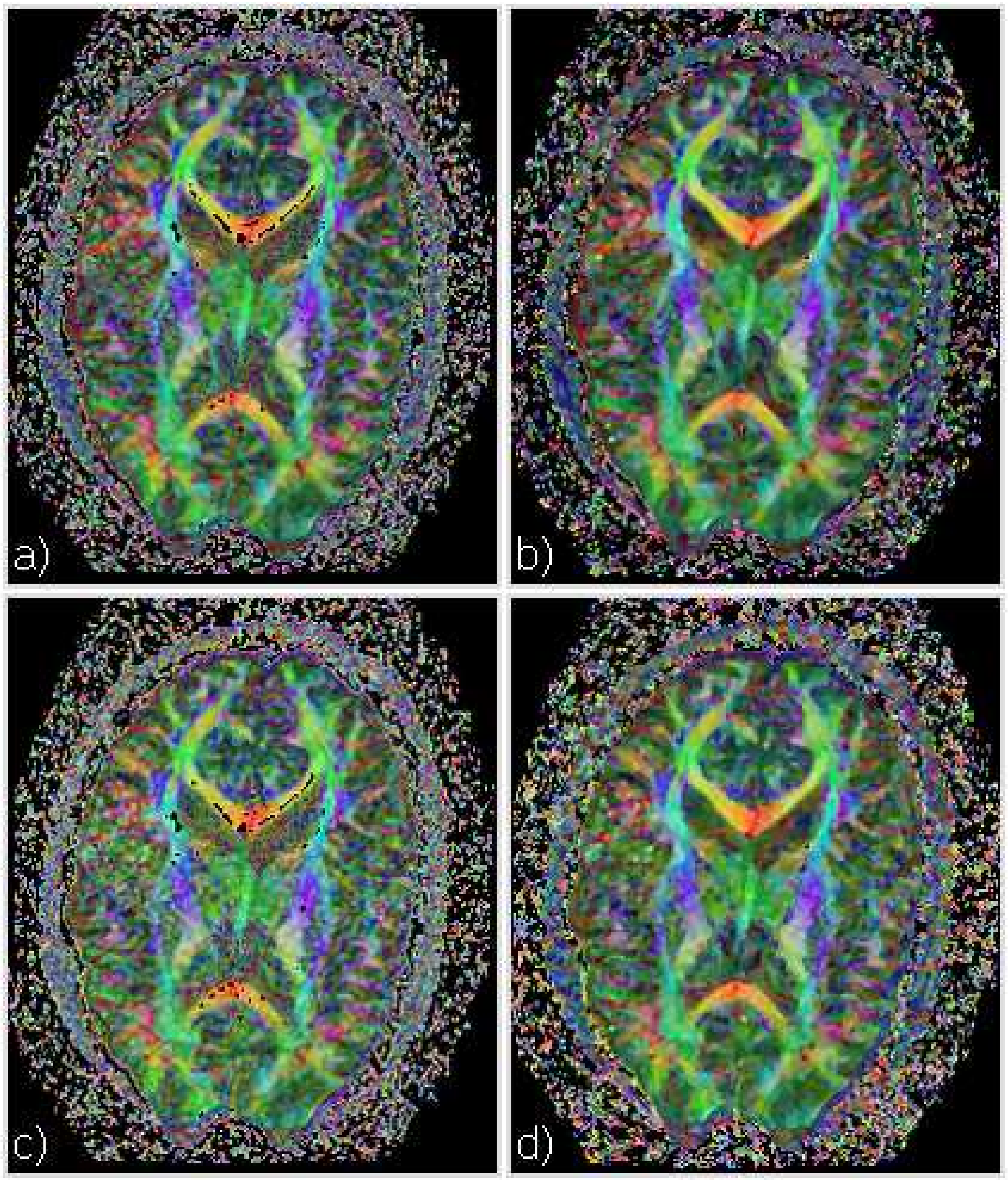

Figure 6: Application of the proposed smoothing algorithm to a brain scan: FA map of an axial slice of the original data using all 55 diffusion weighted images (a). FA map of the smoothed data with the procedure described in the paper (b). FA map of the original data using a reduced set of only 30 diffusion weighted images (c). FA map of the smoothed data with only 30 diffusion weighted images (d). In all images, black regions inside the brain denote areas in which at least one of the eigenvalues was negative.

In other words, we were assuming that neither direction (three components of the diagonalized tensor, the normalized, orthogonal eigenvectors) nor diffusivity (the other three components, the eigenvalues) are favored in applications. Variations by altering the test statistic, Eq. (10), and, subsequently, the statistical penalty, Eq. (14). are possible. For example, for fiber tracking, in which the FA values are used only for thresholding and are of minor importance, could profit from putting more weight onto the estimation of principal tensor directions. Clinical applications, in which subtle between-patients or longitudinal differences between anisotropy or diffusivity values are searched for, may profit from neglecting principal tensor directions. To evaluate the balances between these alternatives will be the scope of future work.

Acknowledgments

This work is supported by the DFG Research Center MATHEON. H.U.V. acknowledges financial support from the Cervical Spine Research Society.

References

[Alexander et al., 2000] Alexander, A., Hasan, K., Kindlmann, G., Parker, D., and Tsuruda, J. (2000). A geometric analysis of diffusion tensor measurements of the human brain. *Magn. Reson. Med.*, 44:283–291.

[Basser et al., 1994a] Basser, P., Mattiello, J., and Bihan, D. L. (1994a). Estimation of the effective self-diffusion tensor from the NMR spin echo. *J. Magn. Res.*, B(103):247–254.

[Basser et al., 1994b] Basser, P., Mattiello, J., and Bihan, D. L. (1994b). MR diffusion tensor spectroscopy and imaging. *Biophysical Journal*, 66:259–267.

[Basser and Pajevic, 2000] Basser, P. and Pajevic, S. (2000). Statistical artefacts in diffusion tensor MRI (DT-MRI) caused by background noise. *Magn. Res. Med.*, 44(1):41–50.

[Bengtsson et al., 2005] Bengtsson, S. et al. (2005). Extensive piano practicing has regionally specific effects on white matter development. *Nature Neuosciene*, 8:1148–1150.

[Bihan et al., 2001] Bihan, D., Mangin, J., Poupon, C., Clark, C., Pappata, S., Molko, N., and Chabriat, H. (2001). Diffusion tensor imaging: Concepts and applications. *J. Magn. Res.*, 13:534–546.

[Bihan and Breton, 1985] Bihan, D. L. and Breton, E. (1985). Imagerie de diffusion in vivo par résonance magnétique nucléaire. *C.R. Acad. Sci. Paris.*, 301:1109–1112.

[Carbon et al., 2004] Carbon, M., Kingsley, P., Su, S., Smith, G. S., Spetsieris, P., Bressman, S., and Eidelberg, D. (2004). Microstructural white matter changes in carriers of the DYT1 gene mutation. *Ann. Neurol.*, 56:283–286.

[Carr and Purcell, 1954] Carr, H. Y. and Purcell, E. M. (1954). Effects of diffusion on free precession in nuclear magnetic resonance experiments. *Physical Review*, 94:630–638.

[Chung et al., 2005] Chung, M., Lee, J., and Alexaender, A. (2005). Anisotropic kernel smoothing in diffusion tensor imaging: theoretical framework. Technical Report TR1109, Department of Statistics, University of Wisconsin-Madison.

[Clark et al., 1999] Clark, C. A., Barker, G. J., and Tofts, P. S. (1999). Magnetic resonance diffusion imaging of the human cervical spinal cord in vivo. *Magn. Reson. Med.*, 41:1269–1273.

[Ding et al., 2005] Ding, Z., Gore, J., and Anderson, A. (2005). Reduction of noise in diffusion tensor images using anisotropic smoothing. *Magn. Res. Med.*, 53(2):485–490.

[Fan, 1996] Fan, J. (1996). Test of significance based on wavelet thresholding and Neyman's truncation. *J. Amer. Statist. Ass.*, 91:674–688.

[Fletcher, 2004] Fletcher, P. T. (2004). *Statistical Variability in Nonlinear Spaces: Application to Shape Analysis and DT-MRI.* PhD thesis, University of North Carolina at Chapel Hill.

[Frank, 2001] Frank, L. (2001). Anisotropy in high angular resolution diffusion-weighted MRI. *Magn. Res. Med.*, 45:935–939.

[Hahn et al., 2006] Hahn, K., Prigarin, S., Heim, S., and Hasan, K. (2006). Random noise in diffusion tensor imaging, its destructive impact and some corrections. In Weickert, J. and Hagen, H., editors, *Visualization and Image Processing of Tensor Fields*, Mathematics and Visualization. Springer, Berlin.

[Heim et al., 2007] Heim, S., Fahrmeir, L., Eilers, P., and Marx, B. (2007). 3D space-varying coefficient models with application to diffusion tensor imaging. *Computational Statistics & Data Analysis.*

[Jones, 2003] Jones, D. K. (2003). When is DT-MRI sampling scheme truly isotropic? *Proceedings of the 11th Annual Meeting of ISMRM*, 11:2118.

[Jones, 2004] Jones, D. K. (2004). The effect of gradient sampling schemes on measures derived from diffusion tensor MRI: A Monte Carlo study. *Magn. Res. Med.*, 51:807–815.

[Khong et al., 2006] Khong, P.-L. et al. (2006). White matter anisotropy in post-treatment childhood cancer survivors: Preliminary evidence of association with neurocognitive function. *J. Clin. Oncology*, 24:884–890.

[Kinglsey, 2006] Kinglsey, P. B. (2006). Introduction to diffusion tensor imaging mathematics: Part iii. tensor calculation, noise, simulations, and optimization. *Concepts in Magnetic Resonance Part A*, 28A:155–179.

[Koltchinskii et al., 2007] Koltchinskii, V., Sakhanenko, L., and Cai, S. (2007). Integral curves of noisy vector fields and statistical problems in diffusion tensor imaging: non-parametric kernel estimation and hypotheses testing. *Annals of Statistics*. to appear.

[Lee et al., 2005] Lee, J., Chung, M., Oakes, T., and Alexander, A. (2005). Anisotropic Gaussian kernel smoothing of DTI data. In *Proceedings of the 13th Annual Meeting of ISMRM*, page 2253.

[Leung et al., 2004] Leung, L. H. T. et al. (2004). White-matter diffusion anisotropy after chemo-irradiation: a statistical parametric mapping study and histogram analysis. *Neuroimage*, 21:261–268.

[Liston et al., 2006] Liston, C., Watts, R., Tottenham, N., Davidson, M. C., Niogi, S., Ulug, A. M., and Casey, B. J. (2006). Frontostriatal microstructure modulates efficient recruitment of cognitive control. *Cereb. Cortex*, 16:553–60.

[Liu et al., 1999] Liu, A., Maldjian, J., Bagley, L., Sinson, G., and R.I., G. (1999). Traumatic brain injury: Diffusion-weighted MR imaging findings. *Am. J. Neuroradiol.*, 20:1636–1641.

[Mattiello et al., 1994] Mattiello, J., Basser, P. J., and Bihan, D. L. (1994). Analytical expressions for the b matrix in NMR diffusion imaging and spectroscopy. *J. Magn. Res.*, A(108):131–141.

[Mattiello et al., 1997] Mattiello, J., Basser, P. J., and Bihan, D. L. (1997). The b matrix in diffusion tensor echo-planar imaging. *Magn. Res. Med.*, 37:292–300.

[McKinstry et al., 2002] McKinstry, M. et al. (2002). Radial organization of developing preterm human cerebral cortex revealed by non-invasive water diffusion anisotropy mri. *Cereb. Cortex.*, 12:1237–1243.

[Melhem et al., 2002] Melhem, E., Mori, S., Mukundan, G., Kraut, M., Pomper, M., and van Zijl, P. (2002). Diffusion tensor MR imaging of the brain and white matter tractography. *Am. J. Radiol.*, 178(1):3–16.

[Merboldt et al., 1985] Merboldt, K., Hanicke, W., and Frahm, J. (1985). Self-diffusion NMR imaging using stimulated echoes. *J. Magn. Res.*, 64:479–486.

[Mori and Zhang, 2006] Mori, S. and Zhang, J. (2006). Principles of diffusion tensor imaging and its applications to basic neuroscience research. *Neuron*, 51:527–539.

[Mukherjee and McKinstry, 2006] Mukherjee, P. and McKinstry, R. (2006). Diffusion tensor imaging and tractography of human brain development. *Neuroimaging Clin. North Am.*, 16:19–43.

[Nakayama et al., 2006] Nakayama, N., Okumura, A., Shinoda, J., Yasokawa, Y. T., Miwa, K., Yoshimura, S. I., and Iwama, T. (2006). Evidence for white matter disruption in traumatic brain injury without macroscopic lesions. *J. Neurol. Neurosurg. Psychiatry*, 77:850–855.

[Neyman, 1937] Neyman, J. (1937). Smooth test for goodness-of-fit. *Skand. Aktuarietidskr.*, 20:149 – 199.

[O'Sullivan et al., 2005] O'Sullivan, M., Barrick, T. R., Morris, R. G., Clark, C. A., and Markus, H. S. (2005). Damage within a network of white matter regions underlies executive dysfunction in CADASIL. *Neurology*, 65:1584–1590.

[Parker et al., 2000] Parker, G., Schnabel, J., Symms, M., Werring, D., and Barker, G. (2000). Nonlinear smoothing for reduction of systematic and random errors in diffusion tensor imaging. *J. Magn. Res. Im.*, 11:702–710.

[Polzehl and Spokoiny, 2006] Polzehl, J. and Spokoiny, V. (2006). Propagation-separation approach for local likelihood estimation. *Probab. Theory and Relat. Fields*, 135:335–362.

[Schneider et al., 2004] Schneider, J. F., Il'yasov, K. A., Hennig, J., and Martin, E. (2004). Fast quantitative diffusion-tensor imaging of cerebral white matter from the neonatal period to adolescence. *Neuroradiology*, 46:258–266.

[Schwartzman et al., 2005] Schwartzman, A., Dougherty, R. F., and Taylor, J. E. (2005). Cross-subject comparison of principal diffusion direction maps. *Magn. Res. Med.*, 53:1423–1431.

[Smith et al., 2006] Smith, S. M. et al. (2006). Tract-based spatial statistics: Voxelwise analysis of multi-subject diffusion data. *Neuroimage*, 31:1487–1505.

[Stejskal and Tanner, 1965] Stejskal, E. and Tanner, J. (1965). Spin diffusion measurements: spin echoes in the presence of a time-dependent field gradient. *J Chem Phys*, 42:288–292.

[Sundgren et al., 2004] Sundgren, P. C., Dong, Q., Gomez-Hassan, D., Mukherji, S. K., Maly, P., and Welsh, R. (2004). Diffusion tensor imaging of the brain: Review of clinical applications. *Neuroradiology*, 46:339–359.

[Tabelow et al., 2006a] Tabelow, K., Polzehl, J., Ulug, A. M., Dyke, J. P., Heier, L. A., and Voss, H. U. (2006a). Accurate localization of functional brain activity using structure adaptive smoothing. Preprint 1119, WIAS.

[Tabelow et al., 2006b] Tabelow, K., Polzehl, J., Voss, H. U., and Spokoiny, V. (2006b). Analyzing fMRI experiments with structural adaptive smoothing procedures. *Neuroimage*, 33:55–62.

[Taylor and Bushell, 1985] Taylor, D. and Bushell, M. (1985). The spatial mapping of translational diffusion coefficients by the NMR imaging technique. *Phys Med Biol*, 30:345–349.

[Tuch et al., 1999] Tuch, D., Weisskoff, R., Belliveau, J., and Wedeen, V. (1999). High angular resolution diffusion imaging of the human brain. In *Proceedings of the 7th Annual Meeting of ISMRM*, page p 321.

[Voss et al., 2007] Voss, H. U., Tabelow, K., Polzehl, J., Tchernichovsky, O., Maul, K. K., Salgado-Commissariat, D., Ballon, D., and Helekar, S. A. (2007). Functional MRI of the zebra finch brain during song stimulation suggests a lateralized response topography. *PNAS*, in press.

[Weickert, 1998] Weickert, J. (1998). *Anisotropic Diffusion in Image Processing*. ECMI. Teubner-Verlag, Stuttgart.

[Weickert, 1999] Weickert, J. (1999). Coherence-enhancing diffusion filtering. *International Journal Computer Vision*, 31:111–127.

[Westin et al., 1999] Westin, C.-F., Maier, S. E., Khidhir, B., Everett, P., Jolesz, F. A., and Kikinis, R. (1999). Image processing for diffusion tensor magnetic resonance imaging. In *Medical Image Computing and Computer-Assisted Intervention*, Lecture Notes in Computer Science, pages 441–452.